Egyptian Journal of Geology

https://egjg.journals.ekb.eg

Application of Remote sensing techniques in discrimination of rock units and preliminary assessment of tectonic activity using ASTER and ALOSE-PALSAR data at Gabal Delihimmi, Central Eastern Desert, Egypt

Abdelrahman Khalifa

Department of Geology, Faculty of Science, Al-Azhar University, Cairo 11884, Egypt

THE CURRENT study examines the validity of remote sensing and tectonic geomorphology techniques in delineating different lithologies and inferring the relative tectonic activity in arid areas. Principle Component Analysis, spectral Band Ratioing, and Minimum Noise Fraction Analysis were applied using the satellite ASTER data of Gabal Delihimmi area in Central Eastern Desert of Egypt. Additionally, mountain front sinuosity and valley floor width to valley height ratio as two major geomorphic indices were extracted and calculated from the ALOSE-PALSAR digital elevation model along 25 different tectonic elements in the study area. Processing of Aster 9 bands facilitates discrimination of Gabal Delihimmi lithologies by updating the recently published map of the study area. The illustration of the diagram based on values of studied mountain front sinuosity and valley floor width to valley height ratio shows three different relative tectonic activity classes: low, moderate, and high. Accordingly, two normal and three strike-slip faults provide a moderate class of tectonic activity while the lowest record of the activity values was observed along the fold that is located in the south-eastern corner of the study area. As a result, in this study, an up-to-date geological map of Gabal Delihimmi area based on the visual interpretation of the processed ASTER data reveals the presence of several geological boundaries and tectonic offsets. This work demonstrates that remote sensing and geomorphic indices are very valuable tools in lithological discrimination and assessing tectonic activity signals and therefore they can be applied successfully to other similar regions where climate is arid and vegetation is rare.

Keywords: Remote sensing, Lithological discrimination, Geomorphic indices, Tectonic activity, Gabal Delihimmi, Eastern Desert, Egypt.

1. Introduction

In the last decades, many researchers have developed and applied modern and advanced algorithms, methods, and techniques in their studies aiming to minimize cost and time and present sufficient answers for various scientific problems. In earth sciences, remote sensing and geospatial analysis techniques have been broadly applied providing important results and models to achieve different goals in different areas. These techniques are used in numerous fields of researches starting from mineral exploration (Sabins 1999), rock discrimination (Mohamed et al. 2021), active tectonics (Khalifa et al. 2019) to environmental geology (Shrestha et al. 2016). ASTER satellite data has considerable advantages as it provides a combination of wide coverage of spectral and high resolution of near-infrared and visible bands (Gad and Kusky 2007). Additionally, analysis of drainage networks along different faults using geospatial analysis techniques presents significant remarks on the evolution of faults and modern-day activities (Khalifa et al. 2018). The study area, comprising

*Corresponding author e-mail: akhalifa@azhar.edu.eg
Received: 27/10/2023; Accepted: 10/11/2023
DOI: 10.21608/EGJG.2023.243614.1059

Gabal Delihimmi, is situated in the Central Eastern Desert within Wadi Um Ghieg block. It is bounded by latitudes 25° 40` N & 25° 48` N and longitudes 34° 17` E & 34° 23` E (Fig. 1). Gabal Delihimmi granitoids pluton or intrusion has a particular significance because it exists as a multistage pluton that is composed of late-collisional rocks. The study of this pluton helps in understanding the presence of some economic materials such as rare-metal granites (Farahat et al. 2011). Farhat et al., (2011) presented new data on geochemistry and petrology expanding the geological information about the Gabal Delihimmi pluton. The study area represents a part of the Neoproterozoic Egyptian Arabian Nubian Shield presenting four major groups: 1) ophiolite, 2) gneiss, 3) igneous intrusions, and 4) Island arc rocks (Asran et al. 2017). Sabet (1961) discriminated Gabal Delihimmi pluton into granodiorite, diorite, and muscovite, whereas Gabal Nusla, located northwest, was mapped as porphyritic granite. The granitic phases and ages of Gabal Delihimmi pluton were discussed and suggested by several studies such as (Akaad and Noweir 1978), (Hamimi 1996), (Akaad, M.K., Abu El Ela 2002), (Hassan and Ramadan 2015). This current study aims to evaluate the validity of ASTER-SWIR processing results in discriminating different varieties of granite that composes Gabal Delhimmi intrusion and delineating the other Neoproterozoic units around it. This present study also targets to examine a combination technique of tectonic geomorphology along the different types of structural elements affecting the study area to provide a preliminary classification of tectonic activity.

2. Geology

The Central Eastern Desert (CED) presents complete crust rocks of the Arabian Nubian Shield (Farahat et al. 2011). A system of Arc-Back-Arc was claimed to be observed in the CED on a subduction zone (Farahat et al. 2010). The geological units of Gabal Delihimmi were recorded and mapped by researchers of the geological surveying authority producing a geological map of Wadi Al Barramiyah at scale 1: 250,000 (EGSMA 1992). They have distinguished the Precambrian units into different rock units: 1) infrastructural rock units; 2) a superstructural rock unit; and 3) intrusive rock units including Delihimmi granitic classes and dykes (Asran et al. 2017) (Fig. 2).

The infrastructural rocks in the Gabal Delihimmi area are represented by Mirifiya granite including a migmatite association, amphibolite, and deformed granitoids. This granite unit is recorded as an oldest rock in the study area (Asran et al. 2017). The Neoproterozoic superstructural basement in the Gabal Delihimmi area was recognized by ophiolitic rock units, island-Arc metavolcanics rocks and metavolcanoclastics. Both ophiolitic and island-arc rock units were metamorphosed deforming the facies of greenschist which were intruded by granitic phases of Gabal Delihimmi (El Gaby et al. 1994). The northern part of Gabal Delihimmi ophiolitic blocks or ophiolitic mélange sheets were deformed and observed enclosing in meta-mudstones rocks (Asran et al. 2017). The composition of metavolcano-clastics and metavolcanics ranges from intermediate to calc-alkaline due to the tectonic setting of the island arc rocks. The intrusion shape of Gabal Delihimmi shows an oval body, 7 km × 15 Km, and thinning southward. It has been observed and mapped within a major anticline form composed of ophiolitic mélange, metavolcanics, and metavolcano-clastics (Asran 1991) and (Asran et al. 2017). Asran et al. 2017 presented detailed petrographic and field information about Gabal Delihimmi suggesting that Gabal Delihimmi intrusion is discriminated into synogranite, monzogranite, granodiorite, and alkali-feldspar granite.

Tectonically, Gabal Delihimmi shows different types of structural elements including shear zones, faults, and folds (Asran et al. 2017). Three main strike groups of shear zones and faults were observed and mapped in the study area from oldest to youngest as NW-SE, NE-SW, and E-W. The NW-SE groups comprise some faults of strike NNW-SSE which were cut by other groups. This group also presents some thrust faults and shear zones. The NE-SW groups that cut the NW-SE strike, were in turn cut by the E-W strike group. They mainly are dextral strike-slip shears with several normal faults. The youngest E-W group presents some ENE-WSW strikes that cut the faults of the two previous groups. They are at most left lateral strike-slip faults recording offsets ranging from 2 m to about 2 km.

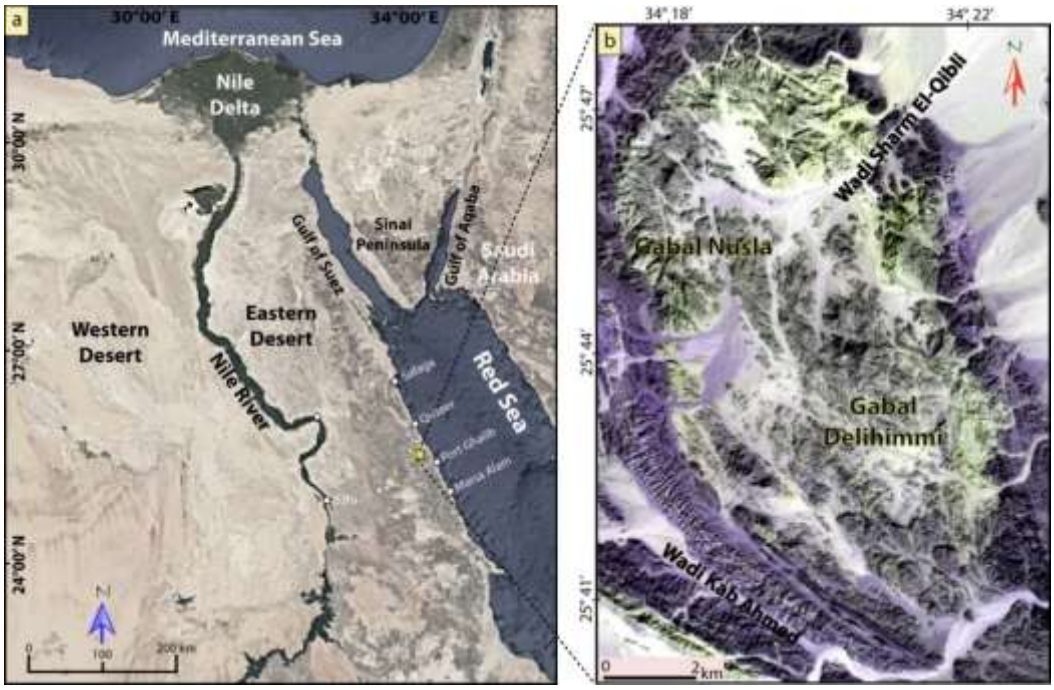

Fig. 1. a) Google earth image of Egypt including Gabal Delihimmi location (Yellow Square). b) ASTER, 742 image of Gabal Delihimmi area.

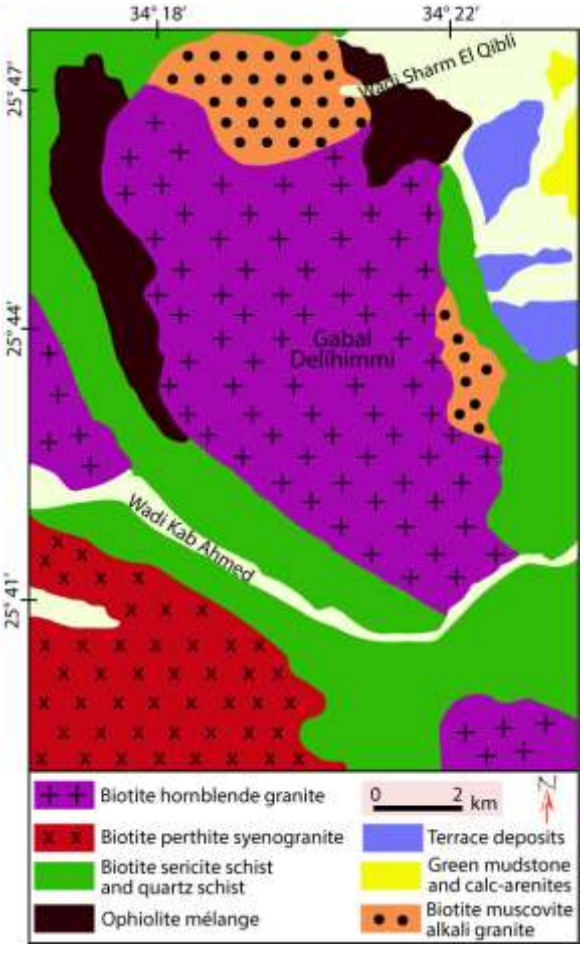

Fig. 2. Geological map of Gabal Delihimmi area in Central Eastern Desert (modified after Asran et al., 2017).

3. Materials and Methods

To best define and assess the different rock types and structural elements of the study pluton, various analysis were performed based on different spectral and spatial data. The data acquisition and processing in this work includes two parts. The first part, is the processing of ASTER data which have been obtained from the USGS website (https://earthexplorer.usgs.gov/). An ASTER L1T scene comprising the study mountain was acquired in May, 2022 (Fig. 3). The image processed in this work has been georeferenced to zone 37 UTM, North projection through the datum WGS-1984. Several essential pre-processing steps have been applied preparing the study area for processes. Because of cross-talk impact of SWIR, the correction of cross-talk was applied directly on the acquired ASTER scene (Khalifa et al. 2020). Layer-stacking and re-sample processes have been applied to combine SWIR and VNIR datasets providing ASTER image with a spatial resolution of 15 m. The study rocks in this work have been discriminated using Principle Component Analysis (PCA), Band Ratio Composite (BRC), and Minimum Noise Fraction (MNF) techniques (Sabins 1999; Asran et al. 2017; Khalifa et al. 2020; Hassan and Ramadan 2015). These techniques are running effectively in arid regions; thus, ASTER data processing is very useful in distinguishing the study rocks of Gabal Delihimmi. ASTER data scene was processed using ENVI 5.4 software package.

The second part includes processing of the ALOSE-PALSAR digital elevation model (DEM) dataset. It was acquired from the NASA Earth data website (https://search.asf.alaska.edu/#/) with a spatial resolution of 12.5 m. Tectonic geomorphology including analysis of river systems provides significant clues about the evolution of faults and current tectonic activity signals (El Hamdouni et al. 2008). In this work, Mountain front-sinuosity and valley floor width-to-valley height ratio indices were applied along the structural elements in the study area. Mountain-front sinuosity index (S_{mf}) helps recognizing the link between erosion and tectonics assigning differences between the straight distance and the real trace of the mountain-front segment (Azor et al. 2002). This index is calculated as:

$$S_{mf} = L_{mf}/L_s$$

where, L_{mf} defines the entire mountain-front length and L_s measures its straight length. The hill-shade map extracted from the geospatial processing was analysed to define this effective index. S_{mf} index was analysed along 24 fronts along different three structural elements. The valley floor width to valley height ratio index (V_f) examines valleys geometries and assigns uplifting or subsidence rates (Baruah et al. 2020). This index is assigned as:

$$V_f = 2V_{fw}/[(E_{ld}-E_{sc}) + (E_{rd}-E_{sc})]$$

where, $V_{fw,}$ $E_{ld,}$ and E_{rd}estimate the width, left wall elevation, and right wall elevation of the studied valley, respectively, and E_{sc} detects the average valley base elevation (El Hamdouni et al. 2008). This index was analyzed due to the drainage patterns of the study area using ArcGIS 10.4 software package. Hydrology tools were run to extract the drainage systems that provide rivers greater than the 4^{th} order using the streams law of Strahler (1964).

4. Results and discussion

4.1 Remote sensing technique and lithological discrimination

Remote sensing applications in lithological discriminations have been widely applied in different regions with different data and techniques. These techniques are used side by side with field observations mapping unmapped and inaccessible regions. Generally, each single rock unit provides its own signatures of reflectance. Therefore, remote sensing techniques aid in discriminating different lithological units due to their different characteristics of reflectance. In this present study, several processing analyses have been applied to trace the lithological boundaries including PCA, BRC, and MNFA. Accordingly, two different processed band combinations images of PCA were produced as (PC4, PC3, and PC6) and (PC1, PC3, PC9) on Red, Green, and Blue (RGB) (Fig. 4 a, b). PCA was applied to provide uncorrelated results by exploring an orthogonal axes new set using nine ASTER SWIR and VNIR bands. This mathematical step is applied simultaneously within image processing procedures transforming some correlated bands into uncollated bands (Hassan and Ramadan 2015). PCA 4, 3, and 6 in addition to PCA 1, 3, and 9 images enhanced the separation between the lithological units in the study area. Discrimination of most units of the study area was easy to delineate by the produced PCA images. Depending on the virtual comparison and interpretation between the two PCA images, serpentine, alkali granite, and chlorite schist units were well-bounded and separated from surrounding exposed lithological units (Fig. 4). The PCA image (PCA 4, 3, and 6) was used with other band ratios by Hasan and Ramadan (2015) to detect two gold bearing alteration zones in the study area in the Eastern Dessert and to define mineral signatures.

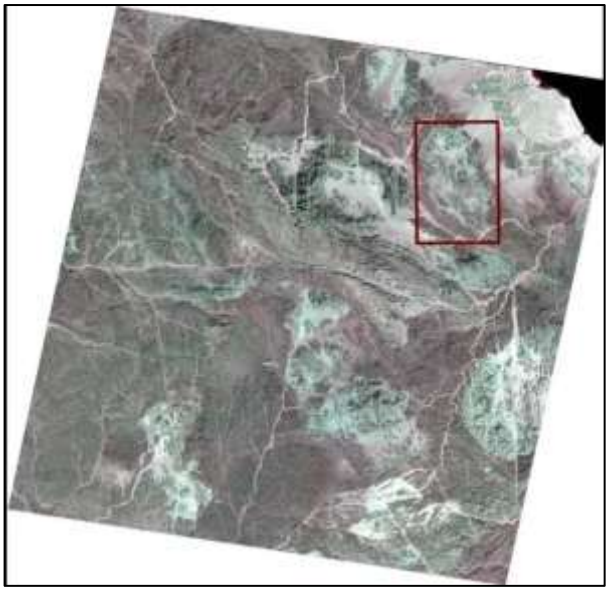

Fig. 3. ASTER L1T scene showing the study area of Gabal Delimmi.

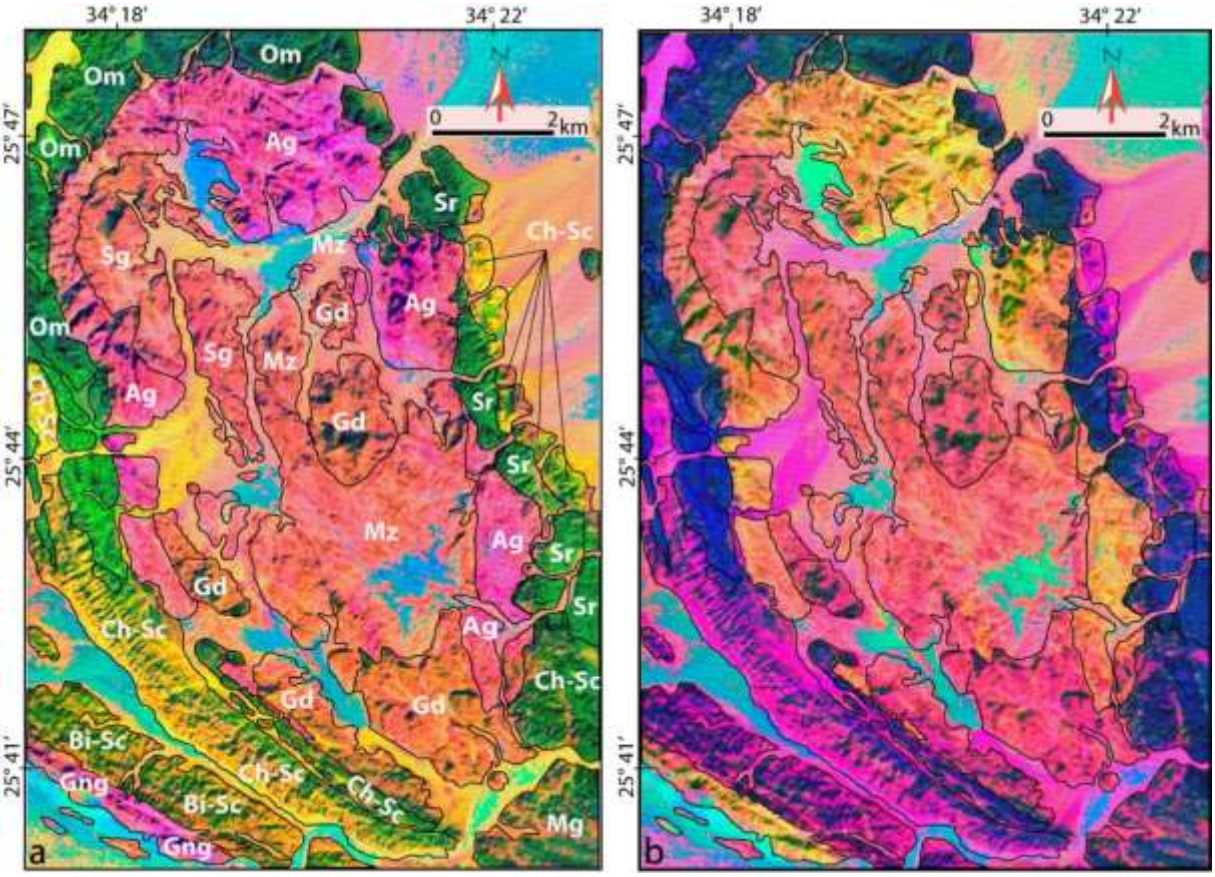

Fig. 4. ASTER principle component images; a) PC4, PC5, and PC6 and b) PC1, PC3, and PC9 in RGB.

ASTER spectral band ratio technique is very useful in mapping different lithological units because it aids in enhancing differences between different bands in addition to its capability to minimize the topographic signals (Inzana et al. 2003). In the current processing, a band ratio of 4/6 was produced first (Fig. 5). Then, ASTER band ratios 6/8, 3/7, and 1/9 was extracted to present the highest factor of optimum index (Fig. 6). Virtual interpretation of this band ratio analysis indicates that this spectral combination presents the best spectral resolution in discrimination of the lithological units and their boundaries in the study area comparing with the other standard band ratios combinations. In this ratio analysis, serpentine units can be easily differentiated from the ophiolitic mélange units providing reddish blue color. Alkali granite units have light yellowish green color, and bi-schist units are dark reddish color. The rest of the lithological units were well-separated by this ratio, thus, it is recommended to apply over areas having similar rock units (Fig. 6). Spectral band ratios analysis (4/7, 4/6, and 4/10) was applied by Gad and Kusky (2007) for mapping granites and metamorphic lithology in Arabian Shield and other similar area.

The MNFA technique was run to define the different dimensionality of the inherent of the nine ASTER different bands segregating and equalizing the data noise and reducing the computational questions for the next processing (Hassan and Ramadan 2015). In this study, MNFA has been used with the nine ASTER SWIR and VNIR bands. Two different ASTER MNF Images were produced namely ASTER MNF (2, 6, and 8) and (4, 5, and 8) in RGB, respectively. The lithological visualization of the resulting MNF 2, 6, and 8 images indicates that every single lithological unit in the study area could be easily separated and bounded, particularly chlorite schist and alkali granite units (Fig. 7). MNFA technique is widely applied for lithological discrimination, particularly in arid regions. For example, the MNFA 2, 4, and 8 image was applied successfully in discriminating two alteration zones in the Eastern Desert of Egypt (Hassan and Ramadan 2015). On the other hand, this technique has proven its validity in tracing and extracting tectonic features and information as well. Khalifa et al. (2021) applied another MNFA image (MNFA 5, 2, and 1) extracted from Landsat 8 satellite data to trace the active

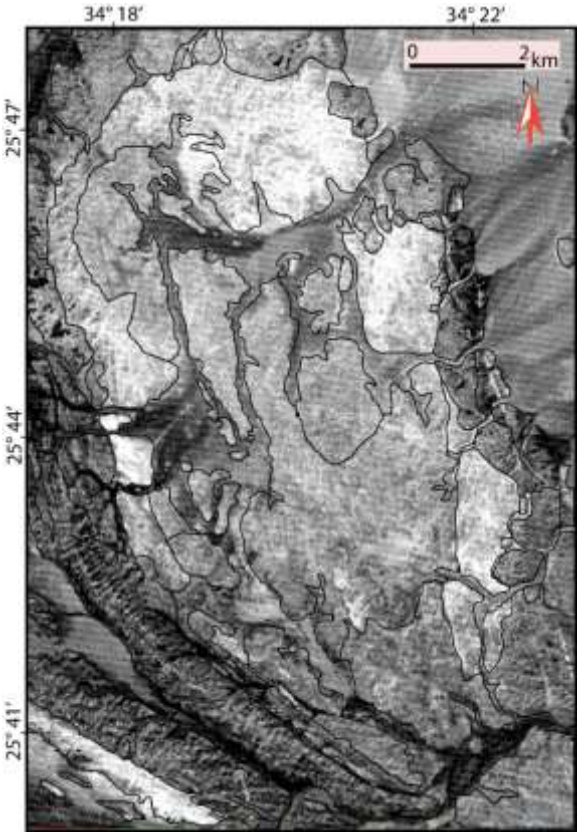

Fig. 5. ASTER grey scale band ratio 4/6 image.

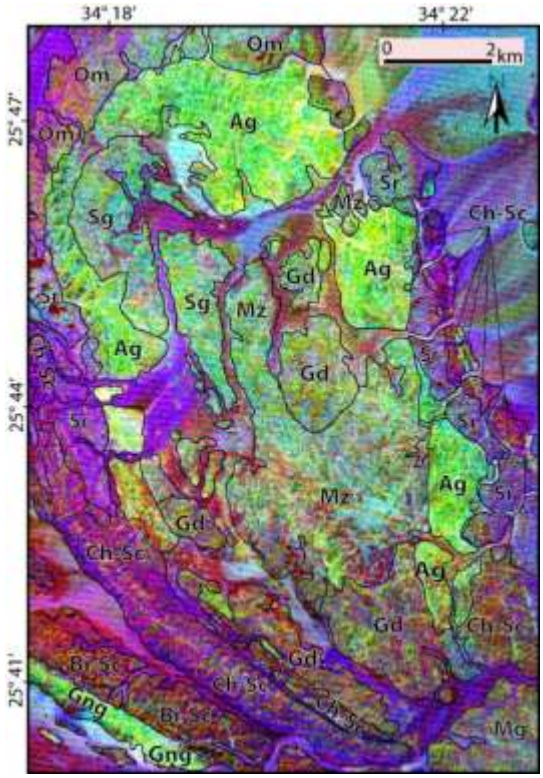

Fig. 6. ASTER band ratios composite 6/8, 3/7, and 1/9 image in RGB.

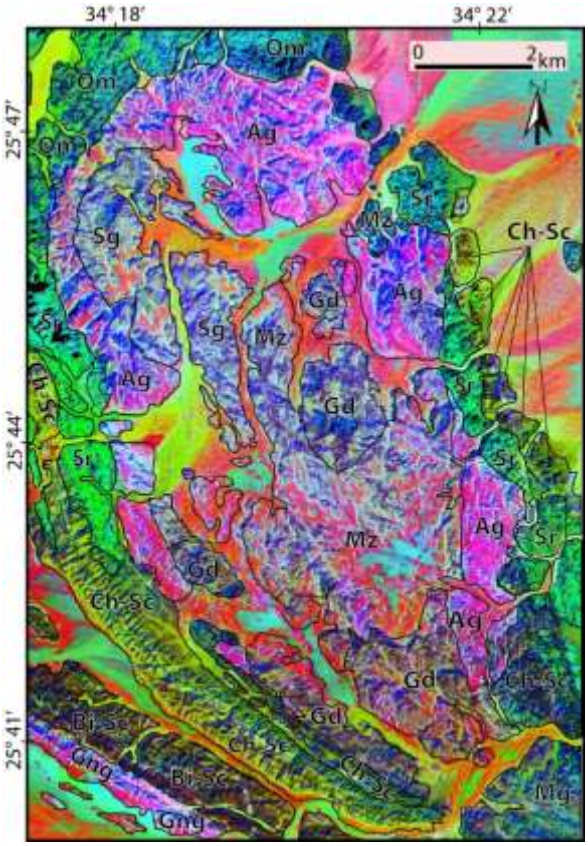

Fig. 7. ASTER minimum noise fraction 2, 6, and 8 image in RGB.

Adıyaman strike-slip fault along the Major transform East Anatolian Fault in Eastern Turkey. In this study, the Minimum Noise Fraction technique was used to trace the tectonic elements in ~~the~~ Gabal Delihimmi area. The MNFA 4, 5, and 8 images in RGB present high relief signatures, which could help in tracing and detecting major tectonic features including normal faults, strike-slip faults, folds, and thrusting (Fig. 8 a, b). A hillshade spectral image extracted from a digital elevation model usually gives important insights into fault tracing and horizontal offsets particularly with active strike-slip faults (Khalifa et al. 2019). In this current study, the PALSAR hillshade map shows weak signatures of the topography and it does not present tectonic offsets.

4.2 Preliminarily relative tectonic activity assessment

Tectonic geomorphology applications present very effective geomorphic indices aiding in providing significant insights into the evolution of different faults through analyzing drainage networks and landforms (El Hamdouni et al. 2008). Mountain front-sinuosity and valley floor width to valley height ratio indices were calculated along 25 mountain segments representing different tectonic elements and trends. The considered mountain fronts Vf locations are shown in Fig 8a, b and could be categorized into four segment groups: 1) fronts along normal faults (fronts 1 and 2); 2) along thrusting (fronts 6, 9, 11, 13, 17, and 18); 3) front along fold axis (front 25); and finally, 4) fronts along strike slip faults including the rest fronts of the study area (Table 1). The mountain front sinuosity values range from 1.5 to 2.98 along the studied different mountain fronts. These results imply that all front segments are active and each tectonic front segment provides its own relief signatures of active uplifting signals. In this study, the lowest value was recorded for front segment 1 (a normal fault) as 1.5, while the highest value was calculated for front segment 21 (fold) as 2.98 (Fig. 9; Table 1). Generally, relatively low values could imply a high rate of tectonic signals (El Hamdouni et al. 2008). Therefore, similar and low values were extracted from segments 21, 7, and 18 indicating higher uplift rates compared to the other segments with low values. While general analysis of S_{mf} geomorphic index does not provide an obvious trend in values in this present study, it gradually ranges from 1.5 and 2.98. The quantitative values of V_f were estimated for the main rivers crossing the proposed mountain fronts of the study area (Fig 8b). The average values of the V_f index range from 0.4 to 1.75 along the 25 segments of fronts (Fig. 9; Table 1). Varying values of this index may depend on basin geometry, discharge of major streams, and lithology type. The lowest values were observed for segments 11, 12, and 20, respectively as 0.4, while the highest value was recorded for front 25. Generally, this index defines valleys as having wide floors and high walls (U shapes), and valleys are characterized by narrow floors and steep walls (V shapes) (Mahmood and Gloaguen 2012). In general, the V_f values are low for most of Gabal Delihimmi area except for some locations in the north-eastern and south-eastern parts of study area.

Table 1. S_{mf} and V_f geomorphic indices of the proposed tectonic segments.

Segments	Type	S_{mf}	V_f
1	Normal fault	1.5	1.7
2	Strike-slip fault	2.6	1.1
3	Normal fault	1.8	1
4	Strike-slip fault	2.4	1
5	Strike-slip fault	2.6	1.6
6	Thrusting	2.65	1.1
7	Strike-slip fault	2.94	1.5
8	Strike-slip fault	2.57	1.6
9	Thrusting	2.7	0.6
10	Strike-slip fault	1.6	1.2
11	Thrusting	2.6	0.4
12	Strike-slip fault	2.7	0.4
13	Thrusting	2.6	2.5
14	Strike-slip fault	2.8	0.7
15	Strike-slip fault	2.65	1.5
16	Strike-slip fault	2.8	0.5
17	Thrusting	2.8	0.5
18	Thrusting	2.9	0.9
19	Strike-slip fault	1.7	0.5
20	Strike-slip fault	2.5	0.4
21	Fold axis	2.98	2
22	Strike-slip fault	2.6	1.6
23	Strike-slip fault	2.7	1
24	Strike-slip fault	2.8	1.5
25	Strike-slip fault	2.8	1.75

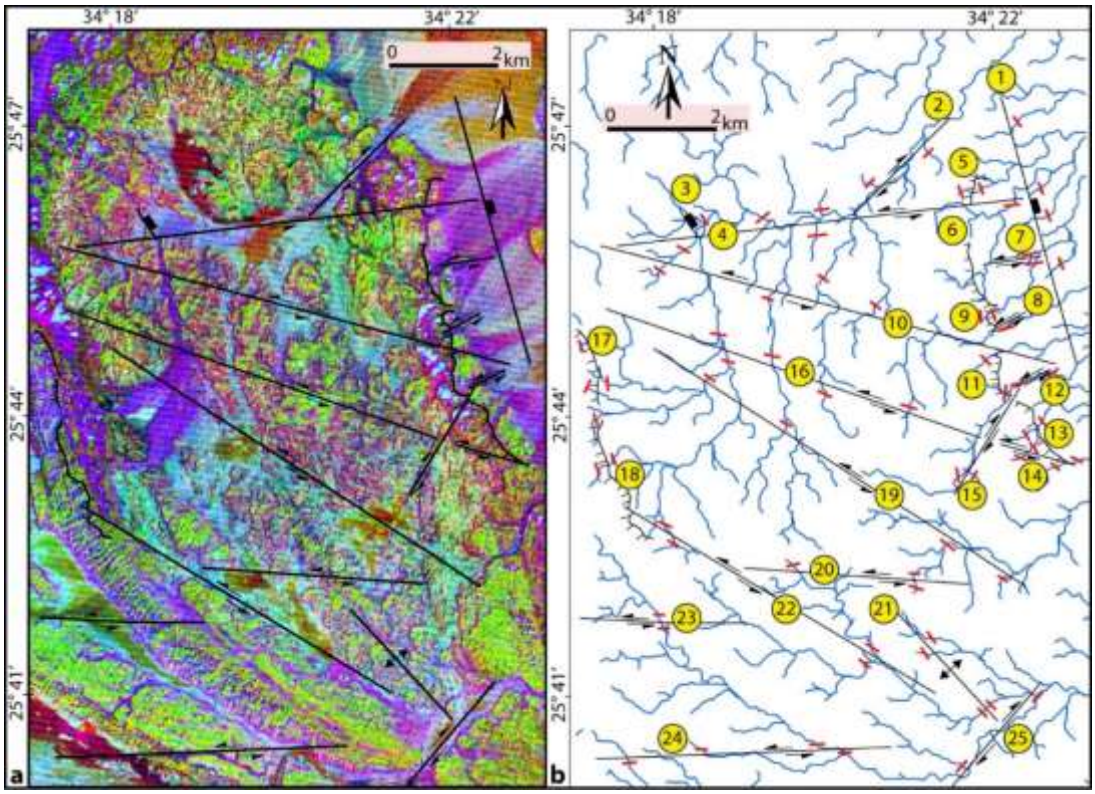

Fig. 8. a) ASTER minimum noise fraction 4, 5, and 8 image in RGB. b) Map showing the traced tectonic elements and extracted drainage water systems, yellow circles indicate tectonic segments numbers and red short lines shows locations of the calculated V_f index.

Various studies applied a combination of S_{mf} and V_f geomorphic indices to simply providing a model of relative tectonic activity levels of different mountain fronts. In many analyses these indices were used and have provided a chart model of different classes of relative tectonic activity (Bull, W.B., McFadden 1977; Silva et al. 2003; Khalifa et al. 2018 and El Hamdouni et al. 2008). In these studies, for example, a chart or diagram model of S_{mf} and V_f quantitative value was illustrated, as a frequency distribution diagram presenting the distribution of these different values along mountain fronts and main rivers. The S_{mf} and V_f values are plotted in one diagram to present a relative of three different tectonic classes of activity levels (El Hamdouni et al. 2008; Khalifa et al. 2018) (Fig. 9). The diagram shows that five tectonic elements including 2 normal faults and 3 strike-slip faults which are represented by segments 1, 3, 4, 10, and 19, respectively were plotted in the moderate zone of the relative tectonic activity classes (class 2). The rest of the segments fall in the low tectonic activity zone of the diagram (class 3).

Therefore, this class can point to that there is no record of any high tectonic activity signals, while moderate signals are recorded mainly in the northern half of the study area. The main cause of these tectonic signal distributions is still unclear, therefore, more tectonic integrations are required to infer the tectonic trend of this area.

4.3 Comparison of the upgrade geological map to the previous published geological map

The new map that has been drawn in this study presents several differences in the delineations and distributions of some lithological units and tectonic offsets compared to the recently published map by Asran et al. (2017). The main differences between the previous map and the updated one are the areas within the black rectangles and dashed polygons, respectively (Fig. 10). For example, in the western part of the study area, a new polygon gave the same spectral signature as the alkali granite unit and it was not mapped in the previously published map. In addition, some of the offsets documented in the previous map, were not extracted ín this current study. For example, at the northern part, a strike-slip fault that 23 that affects chlorite schist units does not show any offsets in this study map although it was traced by a significant offset in the published map. For more clear comparisons, please see rectangles and dashed polygons in Fig. (10).

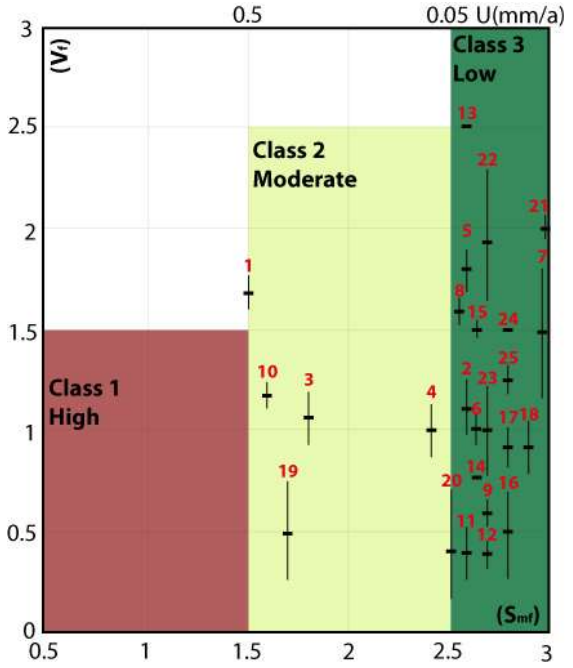

Fig. 9. Plotting of Smf versus V_f for the examined front segments showing tectonic activity classes. Numbers 0.5 and 0.05 at the top indicted uplift rates U (mm/yr), modified from Rockwell et al., (1984).

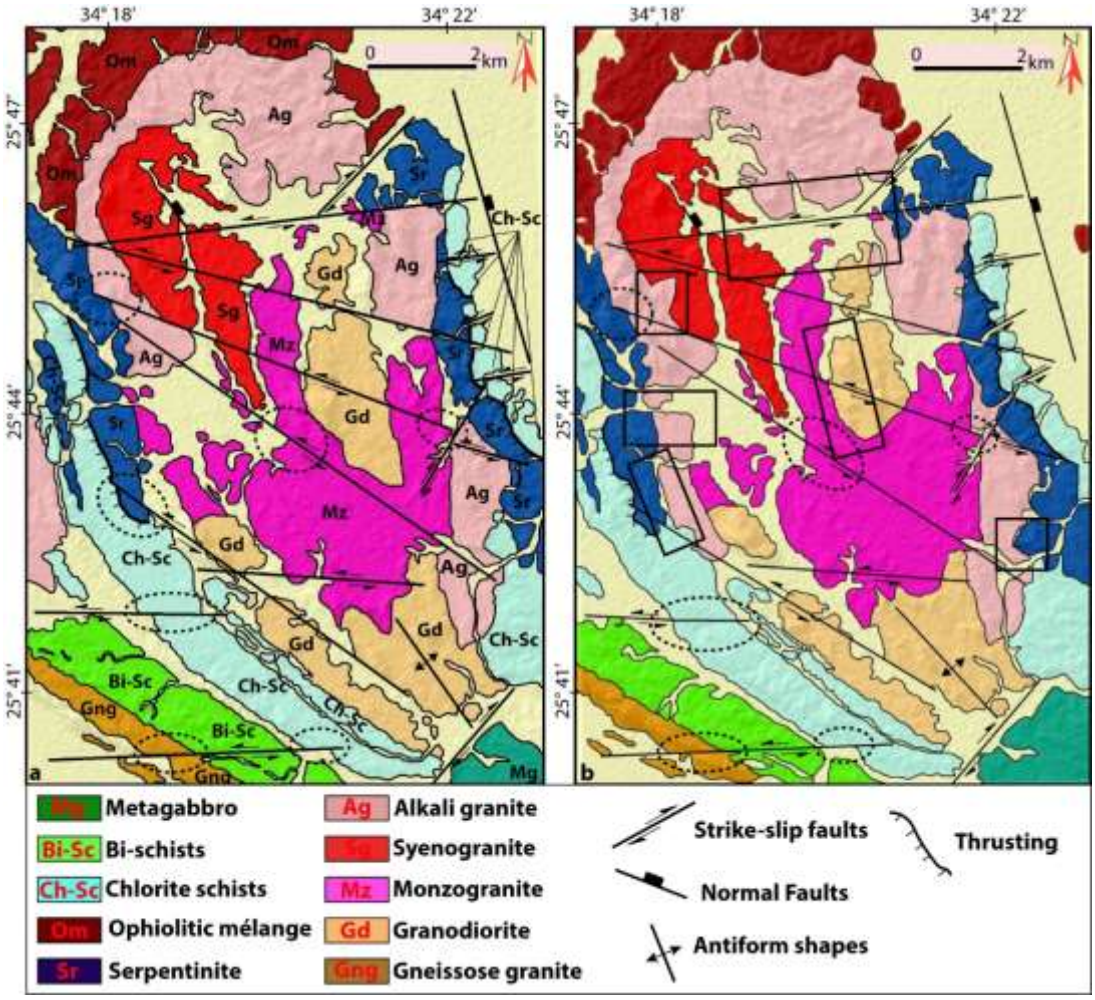

Fig. 10. a) Geological map of the study area published by Asran et al., 2017. b) Readjusted lithological and tectonic map produced by the current study. Black rectangles and dashed polygon indicate differences between the published and new maps.

5. Conclusions

In this study, the Advanced Spaceborne Thermal Emission and Reflection Radiometer (ASTER) data were acquired and processed including Principle Component Analysis, spectral Band Ratio technique, and Minimum Noise Fraction Analysis to investigate and re-map the lithological units of Gabal Delihimmi area in the Central Eastern Desert of Egypt. Additionally, ALOS-PALSAR digital elevation model data was used to extract geomorphic indices including mountain front sinuosity and valley floor width to valley height ratio along the tectonic elements of the study area.

The work results demonstrate that principle component images of bands 436, band ratio composite image of bands 6/8, 3/7, 1/9, and minimum noise fraction image of bands 268 in RGB represent powerful informative images in discriminating and delineating the contacts of the different lithologies in the study area. A minimum noise fraction 458 acted as a high-relief image aiding in tracing most of the tectonic elements in the study area. A quantitative diagram between mountain front sinuosity and valley floor width to valley height ratio geomorphic indices was prepared to plot the values of these two indicative indices along 25 tectonic segments. Results from this part demonstrate that five tectonic elements including two normal faults and three strike-slip faults fell with moderate tectonic activity zone (class 2) while the other 20 tectonic segments were observed within the low zone of tectonic activity (class 3). These results imply that there are no inactive tectonic segments in the study area but there is no record of the high tectonic activity class.

As illustrated in Fig. (10), a new map is suggested and is displayed in detail showing the new delineations of some lithologies and adjusting some horizontal geological offsets along some strike-slip faults. In addition to the remap of some lithology boundaries, this study claim to contradict that some outcrops are different from the published map by Asran et al. (2017). Finally, this present study proves that geological and tectonic studies are necessary to confirm what has been extracted from the remote sensing data.

Conflicts of Interest: The author declares no conflict of interest.

Contribution of Authors: All authors shared in writing, editing and revising the MS and agree to its publication.

Acknowledgement: The author is grateful to Nazik Öğretmen from Centro de Ciências do Mar (CCMAR) Portugal for her critical reading of the manuscript and her comments to improve this work. The author also thanks the editor Dr. Nahla Abd El-Ghaffar for the editorial handling of the manuscript. The author is grateful to the reviewers; their recommendations and comments were very effective to improve this manuscript.

5. References

Akaad MK, Abu El Ela AM (2002). Geology of the basement rocks in the eastern half of the belt between latitudes 25 30° and 26 30°N Central Eastern Desert, Egypt. Egypt Geol Surv Min Authority, Cairo 78:118.

Akaad MK, Noweir AM (1978). Geology and lithostratigraphy of the Arabian desert orogenic belt of Egypt between latitudes 25° 35′ and 26° 30′N. Precambrian Res 6:A6. https://doi.org/10.1016/0301-9268(78)90063-3.

Asran AM (1991). Geology of W.Um Gheig Area, Eastern Desert of Egypt. Ph. D. Thesis, Sohag Assiut University.

Asran AM, Emam A, El-Fakharani A (2017). Geology, structure, geochemistry and ASTER-based mapping of Neoproterozoic Gebel El-Delihimmi granites, Central Eastern Desert of Egypt. Lithos 282–283:358–372. https://doi.org/10.1016/j.lithos.2017.03.022.

Azor A, Keller EA, Yeats RS (2002). Geomorphic indicators of active fold growth: South Mountain-Oak Ridge anticline, Ventura basin, southern California. Bull Geol Soc Am 114:745–753. https://doi.org/10.1130/0016-7606(2002)114<0745:GIOAFG>2.0.CO;2.

Baruah MP, Bezbaruah D, Goswami TK (2020). Active tectonics deduced from geomorphic indices and its implication on economic development of water resources in South-Eastern part of Mikir massif, Assam, India. Geol Ecol Landscapes 00:1–14. https://doi.org/10.1080/24749508.2020.1754705.

Bull WB, McFadden LD (1977). Tectonic geomorphology north and south of the Garlock fault, California. In: Doehring, D.O. (Ed.), Geomorphology in Arid Regions. Proceedings of the Eighth Annual Geomorphology Symposium. State University of New York, Bin. Am J Sci 559–589.

EGSMA (1992). Geological Map of Wadi Al Barramiyah Quadrangle, Egypt, (Scale 1: 250,000).The Egyptian Geological Survey and Mining Authority, Cairo, Egypt.

El-Gaby S, Khudeir AA, Asran AM (1994). Geology and geochemistry of the Pan-African volcano-sedimentary belt at Wadi Um Gheig Eastern Desert, Egypt. Bull Fac Sci Assiut Univ 23:185–219.

El-Hamdouni R, Irigaray C, Fernández T, et al. (2008). Assessment of relative active tectonics, southwest border of the Sierra Nevada (southern Spain).

Geomorphology 96:150–173. https://doi.org/10.1016/j.geomorph.2007.08.004.

Farahat ES, El Mahallawi MM, Hoinkes G et al. (2010). Pillow form morphology of selected Neoproterozoic metavolcanics in the Egyptian Central Eastern Desert and their implications. J African Earth Sci 57:163–168. https://doi.org/10.1016/j.jafrearsci.2009.09.001.

Farahat ES, Zaki R, Hauzenberger C, Sami M (2011). Neoproterozoic calc-alkaline peraluminous granitoids of the Deleihimmi pluton, Central Eastern Desert, Egypt: implications for transition from late- to post-collisional tectonomagmatic evolution in the northern Arabian–Nubian Shield. Geol J 46:544–560. https://doi.org/10.1002/gj.1289.

Gad S, Kusky T (2007). ASTER spectral ratioing for lithological mapping in the Arabian-Nubian shield, the Neoproterozoic Wadi Kid area, Sinai, Egypt. Gondwana Res 11:326–335. https://doi.org/10.1016/j.gr.2006.02.010

Hamimi Z (1996). Tectonic evolution of the shield rocks of Gabal El-Sibai area, Central Eastern Desert, Egypt. Egypt J Geol 40:423–453

Hassan SM, Ramadan TM (2015) Mapping of the late Neoproterozoic Basement rocks and detection of the gold-bearing alteration zones at Abu Marawat-Semna area, Eastern Desert, Egypt using remote sensing data. Arab J Geosci 8:4641–4656. https://doi.org/10.1007/s12517-014-1562-0.

Inzana J, Kusky T, Higgs G, Tucker R (2003). Supervised classifications of Landsat TM band ratio images and Landsat TM band ratio image with radar for geological interpretations of central Madagascar. J African Earth Sci 37:59–72. https://doi.org/10.1016/S0899-5362(03)00071-X.

Khalifa A, Çakir Z, Owen LA, Kaya (2019). Evaluation of the relative tectonic activity of the adıyaman fault within the arabian-anatolian plate boundary (Eastern Turkey). Geol Acta 17:1–17. https://doi.org/10.1344/GeologicaActa2019.17.6.

Khalifa A, Çakir Z, Owen LA, Kaya Ş (2018). Morphotectonic analysis of the East Anatolian Fault, Turkey. Turkish J Earth Sci 27:110–126. https://doi.org/10.3906/yer-1707-16.

Khalifa A, Çakır Z, Kaya Ş, Gabr S (2020). ASTER spectral band ratios for lithological mapping: a case study for measuring geological offset along the Erkenek Segment of the East Anatolian Fault Zone, Turkey. Arab J Geosci 13:. https://doi.org/10.1007/s12517-020-05849-y.

Mahmood SA, Gloaguen R (2012). Appraisal of active tectonics in Hindu Kush: Insights from DEM derived geomorphic indices and drainage analysis. Geosci Front 3:407–428. https://doi.org/10.1016/j.gsf.2011.12.002.

Mohamed MTA, Al-Naimi LS, Mgbeojedo TI, Agoha CC (2021). Geological mapping and mineral prospectivity using remote sensing and GIS in parts of Hamissana, Northeast Sudan. J Pet Explor Prod Technol 11:1123–1138. https://doi.org/10.1007/s13202-021-01115-3.

Sabet, AH (1961). Geology and Mineral Deposits of Gabal El-Sibai Area, Red Sea Hills, Egypt. Leiden State University, The Netherland.

Sabins FF (1999). Remote sensing for mineral exploration. Ore Geol Rev 14:157–183. https://doi.org/10.1016/S0169-1368(99)00007-4.

Shrestha F, Uddin K, Bikash Maharjan S, Ratna Bajracharya S (2016). Application of remote sensing and GIS in environmental monitoring in the Hindu Kush Himalayan region. AIMS Environ Sci 3:646–662. https://doi.org/10.3934/environsci.2016.4.646.

Silva PG, Goy JL, Zazo C, Bardají T (2003). Faulth-generated mountain fronts in southeast Spain: Geomorphologic assessment of tectonic and seismic activity. Geomorphology 50:203–225. https://doi.org/10.1016/S0169-555X(02)00215-5.

Strahler AN (1964). Strahler, A. (1964) Quantitative Geomorphology of Drainage Basins and Channel Networks. ,. In: In: Chow, V., Ed., Handbook of Applied Hydrology, McGraw Hill, New York. New York, pp 439–476.

تطبيق تقنيات الاستشعار من بعد في تمييز الوحدات الصخرية والتقييم المبدئي للنشاط التكتوني باستخدام بيانات ASTER و ALOS-PALSA بمنطقة جبل دلهمي بوسط الصحراء الشرقية

عبدالرحمن خليفة

قسم الجيولوجيا، كلية العلوم، جامعة الأزهر، القاهرة، مصر

تبحث هذة الدراسة في مدى صلاحية تقنيات الاستشعار عن بعد والجيومورفولوجيا التكتونية في إستكشاف وتحديد الصخور المختلفة واستنتاج النشاط التكتوني النسبي في المناطق القاحلة. تم تطبيق تحليل المكونات الأساسية، وتقنية نسبة النطاق الطيفي، وتحليل أجزاء الضوضاء الدنيا باستخدام بيانات القمر الصناعي ASTER لمنطقة جبل الدلهمي في وسط الصحراء الشرقية في مصر. بالإضافة إلى ذلك، تم حساب نسبة انحراف الجبهة الجبلية وعرض قاع الوادي إلى ارتفاع الوادي حيث تم استخراج وحساب مؤشرين جيومورفيين رئيسين من نموذج الارتفاع الرقمي ALOSE-PALSAR على طول 25 عنصرًا تكتونيًا مختلفًا في منطقة الدراسة. تعمل معالجة نطاقات Aster 9 على تسهيل التمييز بين الصخور في جبل الدلهمي من خلال تحديث الخريطة المنشورة مؤخرًا لمنطقة الدراسة. يوضح الشكل البياني المعتمد على علاقة بين قيم انحراف الجبهة الجبلية المدروسة ونسبة عرض قاع الوادي إلى ارتفاع الوادي ثلاث فئات مختلفة للنشاط التكتوني النسبي، وهي منخفضة ومعتدلة وعالية. وبناء على ذلك، فإن الصدوع العادية وثلاثة من الصدوع الانزلاقية تظهر فئة معتدلة من النشاط التكتوني في حين لوحظ أدنى سجل لقيم النشاط على طول الطية الواقعة في الزاوية الجنوبية الشرقية من منطقة الدراسة. ونتيجة لذلك، تنتج هذه الدراسة خريطة جيولوجية حديثة لمنطقة جبل الدلهمي بناءً على التفسير البصري لبيانات ASTER المعالجة عن طريق دراسة الحدود الجيولوجية بين الوحدات الصخرية المختلفة والإزاحات التكتونية. وأخيرًا، أظهر هذا العمل أن أستخدام تقنيات الاستشعار من بعد ودراسة المؤشرات الجيومورفولوجية هي أدوات قيمة للغاية في التمييز الصخري وتقييم إشارات النشاط التكتوني، وبالتالي يمكن تطبيقها بنجاح على مناطق أخرى مماثلة حيث يكون المناخ جافًا والغطاء النباتي نادرًا.